

Mathematical modelling and active control of oscillators Application to buffet and to compressor surge

Alain Le Pourhiet, Michel Corrège, Daniel Caruana
ONERA, 2 av. Édouard-Belin, 31400 Toulouse, France

e-mail : lepour@cert.fr

Keywords : active control, non linearity, oscillator, Van der Pol, buffet, compressor surge

Abstract

In order to obtain a mathematical model of two-dimensional buffet carried out in a wind tunnel, a Van der Pol oscillator has been enhanced with a transfer function identified from measurements. Using a peculiar control engineering technique, the above model has been used to define a control law aiming to suppress the buffet observed on an airfoil in a wind tunnel. The effects of this law proved to conform to the theory, thus validating the principles of this new type of modelling and design. The same method has been applied to the compressors surge, where measurements are simulated from the Greitzer equations ; the first results are very encouraging.

Nomenclature

$u(t)$	input of the oscillator ;
$E(t)$	input of the complete system ;
$f(y)$	non-linear function in the oscillator ;
$G(s)$	linear control transfer function ;
$L(s)$	linear transfer function in the oscillator ;
$N(y_0)$	harmonic gain of $f(s)$ for $y = y_0 \sin \omega t$;
s	Laplace variable ; symbol of derivation with respect to time ;
$R(\omega), I(\omega)$	real and imaginary parts of $[L(j\omega)]^{-1}$;
$y(t)$	output of the oscillator ;
$Y(t)$	output of the complete system ;
z, k, ω_n	coefficients of the Van der Pol oscillator ;
t	time ;
T	symbol of derivation with respect to ω ;
U	feedback control variable ;
$\Phi(s)$	linear transfer function of the equivalent oscillator when control is applied ;

φ	phase of $y(t)$;
ω	frequency (rad/sec) ;
Γ, Ψ	mass flow and pressure variables in the compressor Greitzer model ;
ξ	nondimensional time in the Greitzer model ;
α, β, γ_i	coefficients in the Greitzer model ;
Ψ_{c0}, H, W	coefficients in the Greitzer model.

Subscripts :

A, B	type of the oscillator ;
n	for the natural self-sustained oscillation ;
0	for equilibrium of sinusoidal regime ;
s	for the synchronisation threshold.

1 Introduction

In the absence of precise explanations and of mathematical equations from physics laws to describe some oscillatory phenomenons, it seemed useful to find a mathematical model which could reproduce the observations obtained in the experiments and which could then be used, away from the experiment site, as a tool in the research of control laws. The second order Van der Pol oscillator is one of the most widely-studied models in existence. It is particularly flexible, as all intervening parameters can be standardised. Nevertheless it has to be enhanced with transfer functions upstream and downstream, allowing the effects observed to be reproduced and a reliable mathematical model thus to be identified.

For a best understanding of our original control law synthesis, we present a general description of systems where self-oscillations appear and their

general mathematical modelling using the Van der Pol oscillator. The 2D buffet phenomenon is then described, as well as the test installation, the model and the actuator used in a wind tunnel. The found control law and the experimental results are then presented as well as an other possible application to compressor surge.

2 A theory of oscillators

2.1 Forced oscillation

Let us consider the system of figure 1. It corresponds to the equation

$$[L(s)]^{-1} y + f(y) = u_0 \sin \omega t . \quad (1)$$

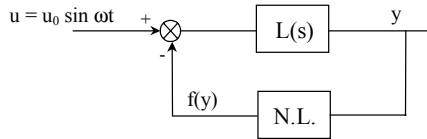


Fig. 1. A diagram describing oscillators.

It is assumed that the linear transfer function $L(s)$ efficiently filters the harmonics above the fundamental ω , thus allowing them to be ignored. We thus have, in established sinusoidal regime,

$$y(t) = y_0 \sin(\omega t + \varphi) \quad (2)$$

with

$$\frac{y_0}{u_0} e^{j\varphi} = \frac{L(j\omega)}{1 + N(y_0)L(j\omega)} . \quad (3)$$

where $N(y_0)$ is the equivalent harmonic gain of the non-linearity $f(y)$; it is supposed not to depend of ω . In the complex plane, $-1/N(y_0)$ is sometimes called the "critical plot". Let us write y and $f[y(t)]$ as

$$y(t) = y_0 \sin(\omega t + \varphi) = V \sin \omega t + W \cos \omega t \quad (4)$$

$$f[y(t)] = q_1(V, W) \sin \omega t + q_2(V, W) \cos \omega t$$

It is shown in references [1-2] that the identification of the coefficients of $\sin(\omega t)$ and $\cos(\omega t)$ in the two sides of (1) leads to

$$e^{\text{Ts}u} M \begin{bmatrix} V \\ W \end{bmatrix} + \begin{bmatrix} q_1(V, W) \\ q_2(V, W) \end{bmatrix} = \begin{bmatrix} u_0 \\ 0 \end{bmatrix} . \quad (5)$$

with

$$u = \begin{bmatrix} 0 & 1 \\ -1 & 0 \end{bmatrix}, \quad M = \begin{bmatrix} R(\omega) & -I(\omega) \\ I(\omega) & R(\omega) \end{bmatrix} .$$

The forced sinusoidal equilibrium (V_0, W_0) is obtained by the operation $s = 0$ in (5), i.e.

$$M \begin{bmatrix} V_0 \\ W_0 \end{bmatrix} + \begin{bmatrix} q_1(V_0, W_0) \\ q_2(V_0, W_0) \end{bmatrix} = \begin{bmatrix} u_0 \\ 0 \end{bmatrix} \quad (6)$$

Let us consider small perturbations (dV, dW) around (V_0, W_0) . We have the linear system

$$[e^{\text{Ts}u} + J_0] \begin{bmatrix} dV \\ dW \end{bmatrix} = 0 \quad (7)$$

with

$$J_0 = \begin{bmatrix} \frac{\partial q_1}{\partial V} & \frac{\partial q_1}{\partial W} \\ \frac{\partial q_2}{\partial V} & \frac{\partial q_2}{\partial W} \end{bmatrix}_{(V=V_0, W=W_0)}$$

The stability of the forced oscillation (V_0, W_0) depends on the roots of the characteristic polynomial

$$P(s) = \det[e^{\text{Ts}u} M + J_0] = \alpha_0 + \alpha_1 s + \alpha_2 s^2 + \dots \quad (8)$$

obtained by expanding the matrix $e^{\text{Ts}u}$ into series. The main coefficients are found to be

$$\alpha_0 = R^2(\omega) + I^2(\omega) + \xi_0 R(\omega) - \eta_0 I(\omega) + \det(J_0) \quad (9)$$

$$\alpha_1 = \frac{dI(\omega)}{d\omega} [2R(\omega) + \xi_0] - \frac{dR(\omega)}{d\omega} [2I(\omega) + \eta_0] \quad (10)$$

with

$$\xi_0 = \left(\frac{\partial q_1}{\partial X} + \frac{\partial q_2}{\partial Y} \right)_0, \quad \eta_0 = \left(\frac{\partial q_1}{\partial Y} - \frac{\partial q_2}{\partial X} \right)_0 .$$

For stability the Routh-Hurwitz criterion must be applied to the α_i coefficients. The highest degree coefficient being positive, a necessary condition is that all the α_i must be positive too ; but with the approximation of slowly varying parameters, we keep only the two first of these conditions. It is shown in [1] that the required inequality $\alpha_0 > 0$ is equivalent to $(dy_0/d\omega) < 0$, i.e. it excludes the solutions between two vertical tangent points of the curve $y_0(\omega)$ plotted for a constant amplitude u_0 . This explains the amplitude jumps of $y(t)$ observed when proceeding at increasing or decreasing frequency. The condition $\alpha_1 > 0$ means a synchronisation threshold for u_0 ; it will be studied later with the Van der Pol oscillator.

2.2 Self-sustained oscillations

If the system is the site of a self-sustained oscillation when $u_0 = 0$, (3) gives

$$L(j\omega) = -\frac{1}{N(y_0)}. \quad (11)$$

Thus a necessary condition required for self-sustained oscillation to exist mathematically is that there is an intersection of the Nyquist plot $L(j\omega)$ with the critical plot $-1/N(y_0)$ in the complex plane. Let ω_n and s_{0n} be the corresponding frequency and amplitude. In the phase plane $(dy/dt, y)$ self-sustained oscillations correspond to stable limit-cycles (see the references [1-9]). The oscillation really exists provided that it is stable. It can be shown that for self-sustained oscillation we have $\alpha_0 = 0$ and that the remaining stability condition $\alpha_1 > 0$ means : *when examining the Nyquist plot of $L(s)$ in the direction of the increasing frequencies, on the left is the direction of the increasing y_0 on the critical plot $-1/N(y_0)$ at their intersection.* This is a known stability criterion for non linear systems.

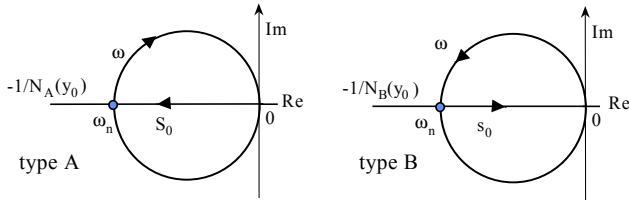


Fig. 2. Nyquist plot and non-linear critical plot for A- and B-type oscillators.

See figure 2. In this way, two types of oscillators are encountered : type A when harmonic equivalent gain $N(y_0)$ is a decreasing function of y_0 , and type B when it is an increasing function of y_0 . One example of type A is the stable transfer function

$$L_A(s) = -\frac{s}{s^2 + 2z\omega_n s + \omega_n^2}$$

associated to $f(y) = k \text{ sign}(y)$ whose the harmonic gain is $N_A(y_0) = 4k/(\pi y_0)$. The critical plot is on the negative real axis. A stable ω_n auto-oscillation thus exists This type of oscillation is seen in systems including saturations.

One example of type B is the unstable linear part

$$L_B(s) = \frac{s}{s^2 - 2z\omega_n s + \omega_n^2}$$

associated to the cubic function $f(y) = ky^3$ whose the harmonic gain is

$$N_B(y_0) = \frac{3}{4}ky_0^2. \quad (12)$$

The critical plot $-1/N_B(y_0)$ is once again on the real

negative axis. The stable ω_n self-sustained oscillation has the amplitude

$$y_{0n} = \sqrt{\frac{-4}{3k\text{Re}[L_B(j\omega_n)]}} = \sqrt{\frac{8z\omega_n}{3k}}. \quad (13)$$

This oscillator is known as a "Van der Pol" oscillator. For the cubic non-linearity we have

$$\sin^3 \omega t = 0.75 \sin(\omega t) - 0.25 \sin(3\omega t)$$

The third harmonic is three times smaller than the first. It is attenuated even more by the linear filter $L(s)$ and this reinforces the first harmonic approximation on which everything we have said so far is based.

2.3 The Van der Pol oscillator

The above B-type oscillator is used to describe numerous natural phenomena. It is equivalent to the well known Van der Pol equation

$$\ddot{y} - 2z\omega_n \dot{y} + \omega_n^2 y + 3ky^2 \dot{y} = u_0 \omega \cos \omega t \quad (14)$$

Carrying (4) into (14) we find the ω sinusoidal regime

$$\rho [\sigma^2 + (\rho - 1)^2] = A^2 \quad (15)$$

with the non dimensional variables :

$$\rho = \frac{3k}{8z\omega_n} (V_0^2 + W_0^2) = \frac{3k}{8z\omega_n} y_0^2 = \left(\frac{y_0}{y_{0n}} \right)^2, \quad (16)$$

$$A^2 = \frac{3ku_0^2}{32z^3\omega_n^3}, \quad (17)$$

$$\sigma = \frac{\omega^2 - \omega_n^2}{2z\omega\omega_n}. \quad (18)$$

The self-sustained oscillation corresponds to $\sigma = 0$, $A^2 = 0$ and $\rho = 1$. In figure 3 the curves $\rho(\sigma)$ are plotted for different values of A^2 . The conditions of stability $\alpha_0 > 0$ and $\alpha_1 > 0$ given by the above method can be written respectively

$$(3\rho - 1)(\rho - 1) + \sigma^2 > 0 \quad (19)$$

$$\rho > 0.5. \quad (20)$$

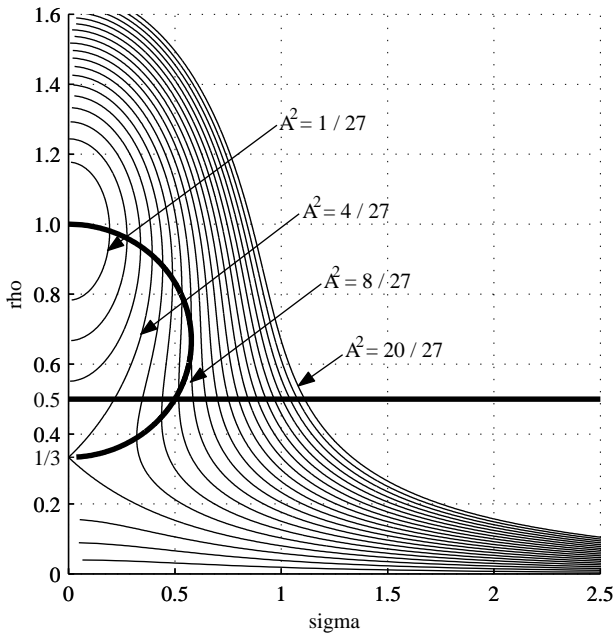


Fig. 3. Van der Pol oscillator : ρ vs σ and A^2 .

The ellipse $(3\rho - 1)(\rho - 1) + \sigma^2 = 0$ is the locus of the points with vertical tangents of the curves $\rho(\sigma)$ for all the A^2 . (19) means a saddle instability inside this “jump” ellipse. (20) corresponds to unstable focus that are due to a residual ω_n self-oscillation ; such a focus is a stable ω_n limit cycle in the (V, W) plane. For details about the kinds of instability, see references [5-10]. Clearly, since ρ is an increasing function of A^2 outside the ellipse, (20) expresses the existence of a threshold for A^2 (and thus for u_0) below which the ω forced oscillation cannot appear alone, its amplitude and frequency remaining confused by the residual ω_n self-oscillation. Above this threshold, the ω_n frequency is muffled and only the ω frequency remains. The synchronisation threshold e_{0s} is obtained by carrying $\rho = 0.5$ into (15) and (17) :

$$u_{0s} = \frac{2}{\omega} \sqrt{\frac{z\omega_n}{3k} [\omega^4 + \omega_n^4 - \omega^2\omega_n^2(2 - z^2)]} = z\omega_n y_{0n} \sqrt{2\sigma^2 + \frac{1}{2}} \quad (21)$$

Inside the jump ellipse, approximately for $\sigma < 0.5$, the forced oscillation is unstable, and the calculation of the synchronisation threshold has to be made using the new boundary of stability, i.e. the upper part of the ellipse ; when ω is near from ω_n , we find

$$u_{0s} = 2y_{0n} |\omega - \omega_n|. \quad (22)$$

For the self-oscillation frequency ($\omega = \omega_n$) the synchronisation threshold is obviously zero.

2.4 Mathematical modelling of experimental results

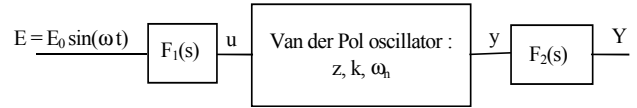


Fig. 4. General mathematical model.

See figure 4. To find a mathematical model of measured oscillations, let us consider a Van der Pol oscillator equipped with the linear transfer functions $F_1(s)$ and $F_2(s)$, upstream and downstream. These functions, as well as the parameters ω_n , z and k of the oscillator, have to be identified together so that the amplitude and the phase of $Y(t)$ coincide as well as possible with measurements corresponding to same inputs $E = E_0 \sin\omega t$. The natural frequency ω_n is known. For given E_0 , z , ω , and $F_1(s)$ we have $u_0 = E_0 \|F_1(j\omega)\|$; then (17) gives A^2 , (15) gives ρ , (16) gives y_0 ; at last the complex gain of the oscillator is computed by (3) :

$$\frac{y_0}{u_0} e^{j\varphi} = \frac{L(j\omega)}{1 + 0.75ky_0^2 L(j\omega)} \equiv H(y_0, j\omega). \quad (23)$$

Let $Y_{mes} \sin(\omega t + \varphi_{mes})$ be the first harmonic of the measured signal $Y(t)$. From the complex identity $F_2(j\omega) = \frac{Y}{y} = \frac{Y}{E} \left(\frac{y}{u} \right)$ we get finally :

$$\|F_2(j\omega)\| = \frac{S_{mes}}{U_0} \frac{1}{\|H(y_0, j\omega)\|} \frac{1}{\|F_1(j\omega)\|}, \quad (24)$$

$$\arg[F_2(j\omega)] = \varphi_{mes} - \arg[H(y_0, j\omega)] - \arg[F_1(j\omega)] \quad (25)$$

The identification of $F_1(s)$ is mainly concerned with the adjustment of the synchronisation threshold. When $F_2(s)$ is found from (24) and (25), the relations $Y_{0n} = \|F_2(j\omega_n)\| y_{0n}$ and (13) give the new value z/k :

$$\frac{z}{k} = \frac{3}{8\omega_n} \left[\frac{Y_{0n}}{\|F_2(j\omega_n)\|} \right]^2. \quad (26)$$

So we do again all the previous calculations until the convergence of z/k . The mathematical model is then a good image of the experimental reality, and it can be used now, more easily than costly experiments, to elaborate an active control law.

3 Synthesis of a control law

With no input ($E = 0$), the system is the site of a self-oscillation which we aim to suppress with a negative feedback transfer function $G(s)$ like in figure 5-a. For a sinusoidal regime the complex gain is now

$$\frac{Y(j\omega)}{E(j\omega)} = F_1(j\omega) \frac{\Phi(j\omega)}{1 + N(y_0)\Phi(j\omega)} F_2(j\omega).$$

with

$$\Phi(s) = \frac{L(s)}{1 + G(s)L(s)F_1(s)F_2(s)}. \quad (27)$$

It is easy to see that the system in figure 5-b is the same that in figure 5-a ; clearly it is a new oscillator like in figure 4 and it happens that it is no longer $L(s)$ which is now with the negative feedback $f(y)$, but the new transfer function $\Phi(s)$.

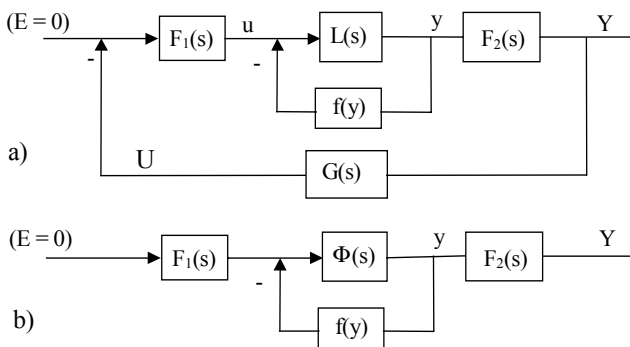


Fig. 5. a) System looped in feedback by a control transfer function $G(s)$. b) Equivalent system.

To muffle the oscillation, $G(s)$ has to be chosen so that the new equivalent system can be made to be no longer a B-type oscillator as defined earlier. Thus $G(s)$ will be such that the Nyquist plot of $\Phi(s)$ shall never cut the negative part of the real axis on which the non-linear critical plot $-1/N(y_0)$ is situated. In other words, the phase of $\Phi(j\omega)$ must never be equal to π , whatever the frequency. A sufficient condition for the phase of a transfer function never to equal π is that this function be stable (i.e. no root of the denominator should have positive real part) and that its relative degree does not exceed 2. Taking into account the difference of degrees, we have the following fundamental result : *if the linear transfer function $\Phi(s)$ is stable, then the self-sustained oscillation cannot exist.* (27) shows that $\Phi(s)$ is equivalent to

$L(s)$ looped in feedback by $G(s)F_1(s)F_2(s)$; so, for $\Phi(s)$ to be stable, it is known that the Nichols plot of $G(s)L(s)F_1(s)F_2(s)$ (gain vs phase) must leave the critical point ($\pm 180^\circ, 0$ db) to the right when it is followed in the direction of the increasing frequencies (see reference [9]). When there are unknown parasite gains and phases, due to error parameters or measurements, gain and phase margins must be large enough so that the critical point remains on the right side. Moreover we will impose all the roots of the denominator of $G(s)$ to have negative real part (this stability is not essential, but it is better for safety). We impose also the difference of degree between the denominator and the numerator to be greater or equal to zero, so that the transfer $G(s)$ is physically possible.

4 Application to buffet

In transonic flow conditions, the shock wave/turbulent boundary layer interaction and flow separations, which induce flow instabilities, “buffet”, and then structure vibrations, “buffeting”, can have an important influence on the behavior of an aircraft. The “buffet” appears at high lift coefficient when the Mach number or the angle of attack increases. This phenomenon limits the flight envelope. The objectives of our active control are to decrease the aerodynamic instabilities due to this type of flow. The used system is a new moving part located at the trailing edge of the wing, the “Trailing Edge Deflector”, designed at ONERA. For more details about the test installation, see the appendix and the references [10-13]

4.1 Identification of the mathematical model

For identification we have used 15 available tests in forced sinusoidal regime with frequencies of 60, 70, 80, 90 and 100 Hz and with E_0 amplitudes of 2.5, 5 and 10 degrees (fig. 4). Whatever the frequency, the synchronisation threshold is always within the 2.5 to 5 range. Below this threshold, beatings are observed with both ω_n and ω frequencies (figure 6).

We also have free tests ($E_0 = 0$) for which the system is self-oscillating at the natural frequency 80 Hz as it is shown on figure 10. It is this oscillation (i.e. the buffet) which we aim to eliminate here.

The identification of $F_1(s)$ is mainly concerned with the adjustment of the synchronisation threshold, but it is convenient here to choose $F_1(s) = 1$ since a small

error only is made here on the synchronisation threshold. Moreover we hope that this error will later be absorbed by sufficient stability margins when the control is developed further. Using a suitable program, the relations (24) and (25) allows then to identify $F_2(s)$:

$$F_2(s) = \frac{1.45 \cdot 10^1 s^3 - 7.35 \cdot 10^2 s^2 + 3.29 \cdot 10^6 s - 6.75 \cdot 10^8}{s^3 + 5.20 \cdot 10^3 s^2 + 1.09 \cdot 10^6 s + 9.26 \cdot 10^8}$$

The roots of the denominator have negative real part since we identify an obviously stable system. The figure 7 gives the gain and the phase of $F_2(j\omega)$ vs ω as well as the experimental points deduced from (24) and (25) for $E_0 = 5$ and $E_0 = 10$ (the value 2.5 is excluded because it is under the synchronised threshold). These two families does not coincide exactly ; it would be possible to choose better functions $f(y)$ and $L(s)$ in order to minimise this difference. Nevertheless the result is fairly satisfactory.

The value of $\omega_n/2\pi$ is obviously the frequency of the free oscillation (= 80 Hz). The measured amplitude is $Y_{0n} = 0.023$. The parameter z/k , determined from (25), is $z/k = 5 \cdot 10^{-7}$. For $E_0 < E_{0s}$, a good coincidence of $Y(t)$ with measurements is found with $z = 0.027$ and $k = 54000$. The theoretical and experimental synchronisation thresholds are shown in figure 8 ; their coincidence is excellent too.

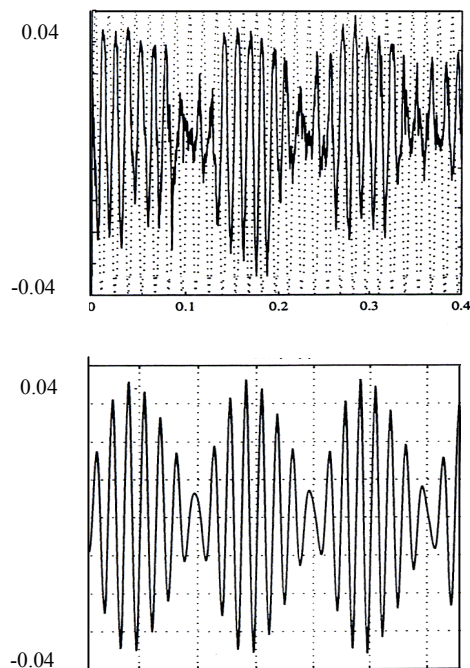


Fig. 6. $E_0 = 2.5$ and $2\pi/\omega = 70$ Hz : beatings observed and simulated with the Van der Pol oscillator.

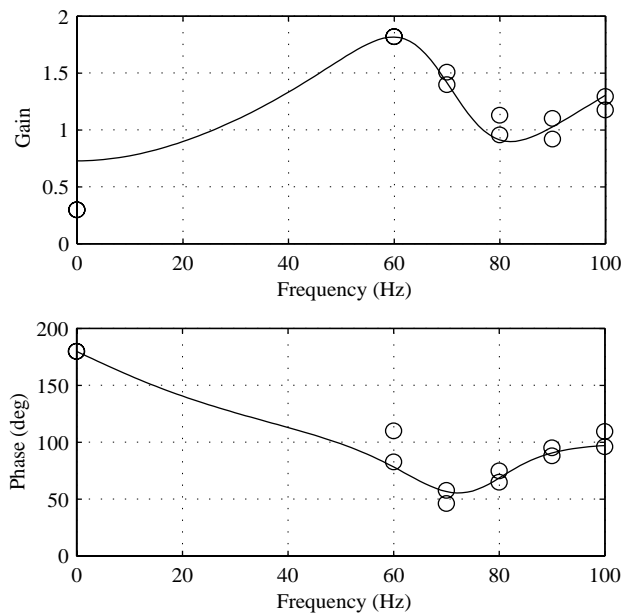


Fig. 7. Identification of the $F_2(s)$ frequency response

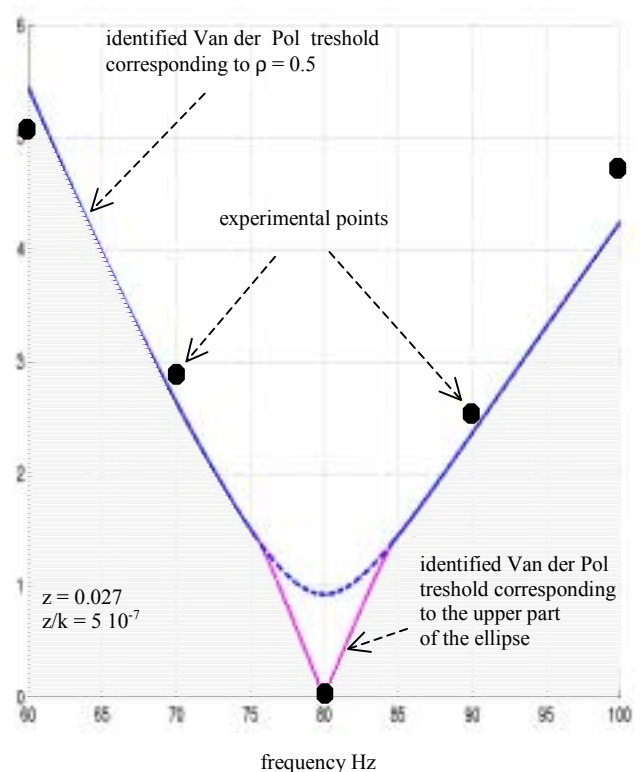


Fig. 8. Synchronisation threshold.

4.2 Control laws

Using a suitable algorithm, a lot of $G(s)$ functions have been found which take into account the previous constraints. The two below are particularly efficient :

$$1) G_1(s) = \frac{4.81 \cdot 10^7 s^2 + 8.72 \cdot 10^9 s + 8.86 \cdot 10^{12}}{s^4 + 8.88 \cdot 10^2 s^3 + 4.79 \cdot 10^5 s^2 + 2.07 \cdot 10^8 s + 3.18 \cdot 10^{10}}$$

To figure 9-a we give the Nichols plot of $L(s)G_1(s)F_2(s)$ and a time simulation. The time simulation shows the instability of the Van der Pol oscillator at zero (due to the negative damping of its linear part), followed by the appearance of self-sustained oscillation ; this oscillation means an overall stability due to the positive damping caused by the non-linearity at high amplitudes. The control $U = G_1 Y$ is applied at time 0.7 second ; the self-sustained oscillation is then immediately and spectacularly muffled.

$$2) G_2(s) = 95 e^{-0.2T_n s} \quad (T_n = 2\pi / \omega_n)$$

This pure delay control has been found experimentally on the wind tunnel. By its Padé approximation, we can verify that it is equivalent to a rational fraction respecting the imposed constraints. The same results as above are given in figure 9-b. Figure 10 shows the experimental self-sustained oscillation before application of control, and the residue measured afterwards ; the frequency analysis of these two signals is also shown, as well as the control time signal. These experiment results are close to those predicted by the theory.

As seen in figure 9-a, the $G_1(s)$ phase margin is $\phi = 65^\circ$ and corresponds to $F_m = 95$ Hz ; for $G_2(s)$ we have 90° and 125 Hz. In both cases, the maximum time delay $\phi/(360 F_m)$ is found to be about $1.8 \cdot 10^{-3}$ second ; this is very large in comparison of the measurements sampling rate and is thus quite satisfactory for safety.

The mathematical model is a convenient assembly of two parts, the oscillator and the identified transfer function $F_2(s)$. It is not possible to consider any internal disturbance which may occur, without greater study of the physical reality of this model. For input and output sinusoidal disturbances, i.e. added in the closed loop of the figure 5-a just before $F_1(s)$ and just after $F_2(s)$, the figure 11 give the gains of the system with feedback controls $G_1(s)$, $G_2(s)$ and $G(s) = 0$. It can be seen that the gain around the resonance is the best with the function $G_1(s)$. This is quite normal since the relative degree of $G_1(s)$ is 2, which guarantees a filtering that does not exist with the pure delay $G_2(s)$, whose gain, always equal to 95, is independent of the frequency.

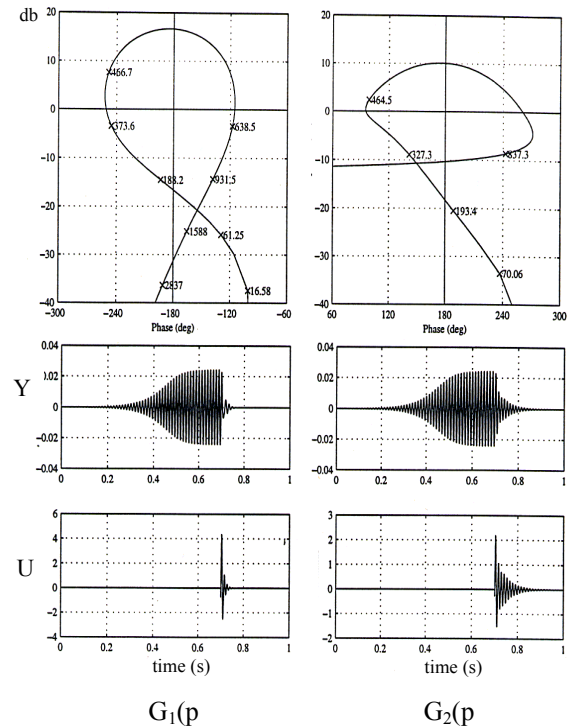


Fig. 9. Nichols plot of $L(s)G_i(s)F_2(s)$, output and control signals.

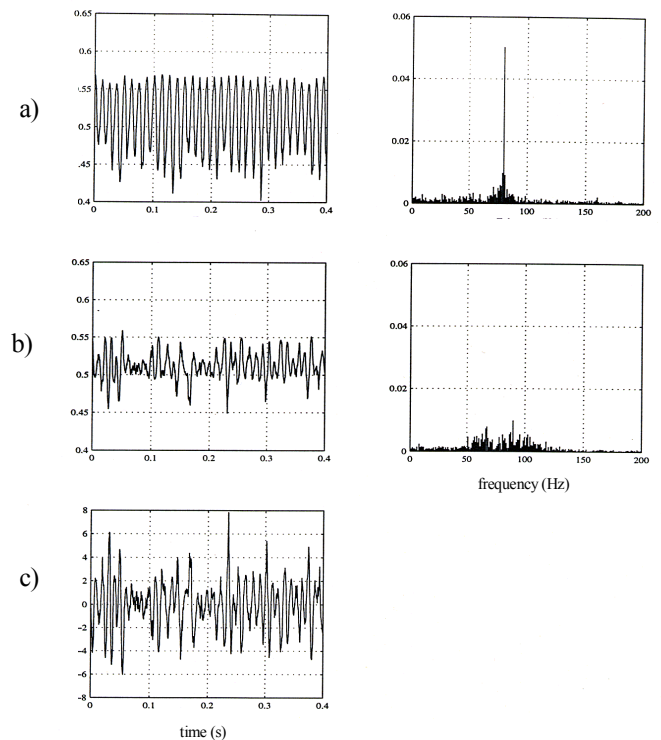


Fig. 10 - Measured signals : a) Output without control. b) Output with control $G_2(s)$. c) Control signal.

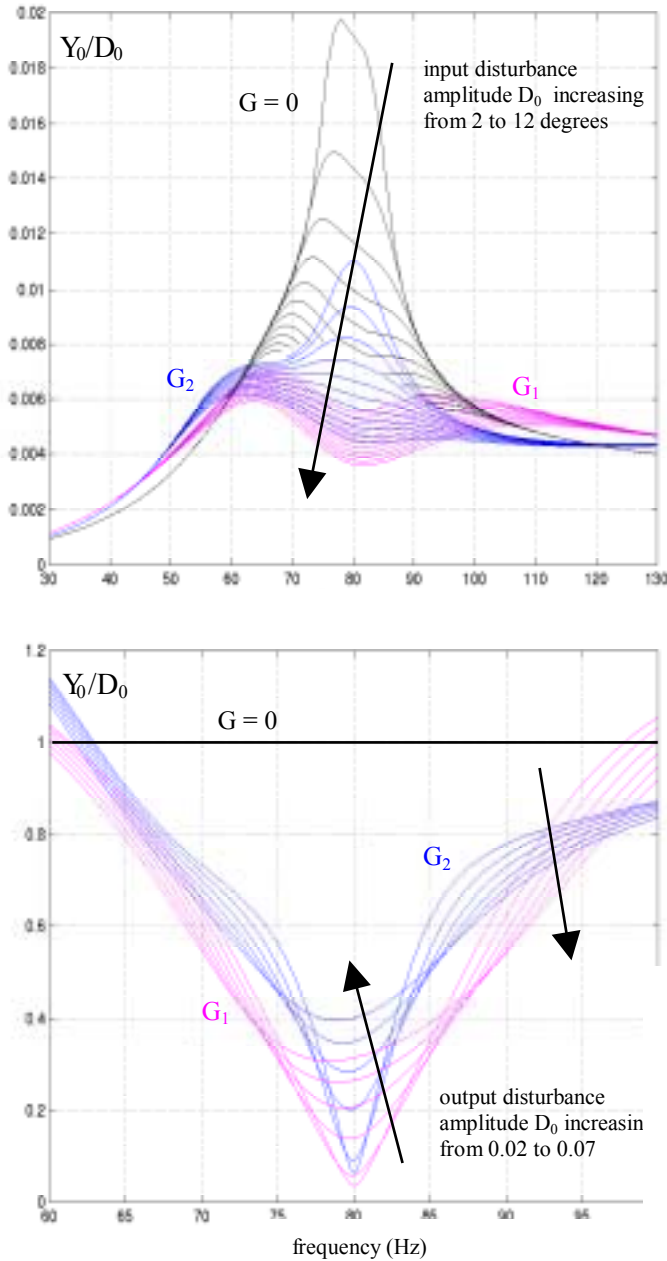


Fig. 11. Closed loop gain for disturbances $D_0 \sin \omega t$.

5 Application to compressor surge

We do not have experimental measurements of an axial flow compressor surge. Thus we use the Greitzer equations to simulate the measurements :

$$\begin{cases} \frac{d\Gamma}{d\xi} = \alpha [\Psi_c(\Gamma) - \Psi + E - U] \\ \frac{d\Psi}{d\xi} = \beta [\Gamma - \Gamma_T(\Psi)] \end{cases} \quad (28)$$

with

$$\Psi_c(\Gamma) = \Psi_{c0} + H \left(1 + \frac{3}{2} X - \frac{1}{2} X^3 \right), \quad (29)$$

$$\Gamma_T(\Psi) = \gamma_t \sqrt{\Psi}, \quad (30)$$

$$X = \frac{\Gamma}{W} - 1. \quad (31)$$

$\Psi_c(\Gamma)$ is the compressor characteristic, $\Gamma_T(\Psi)$ the throttle characteristic. For a complete analysis of these equations, and for others synthesis of control laws, see references [14-17]. When $E = 0$ and for convenient numerical values of the Greitzer model coefficients, self-oscillations (surge) appear. Numerous simulations of forced oscillations ($E = E_0 \sin \omega t$) are used instead true measurements to identify an equivalent Van der Pol model like it was done previously with buffet. The same theory has been applied and an efficient control function $G(s)$ has been found to suppress the surge. This success is quite normal since the Greitzer model is close to a Van der Pol oscillator (it is an exact one for $\gamma_t = 0$). In order to have a zero control signal at the equilibrium, the control law has been enhanced here with the following auto-adaptation :

$$U(s) = G(s)[\Gamma(s) - \bar{\Gamma}(s)] \quad , \quad \bar{\Gamma}(s) = \frac{k}{s(1 + \tau s)} U(s).$$

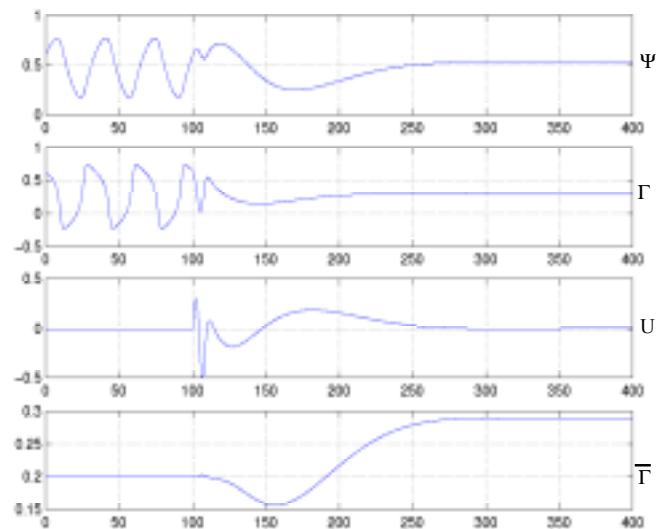


Fig. 12. Control of a compressor surge. The control is applied at time 100.

6 Conclusions

This paper has presented an original method for finding active control laws aiming to suppress self-oscillations encountered in engineering. The success on the 2D aerodynamic buffet, as well as the first results on the control of compressor surge, opens an interesting range of applications for this theoretical study.

APPENDIX

Aerodynamic studies on stiff 2D airfoil, conducted by ONERA, were performed to analyze the effect of the control system on the instabilities. See the references [10-13] for a complete description.

Tests were carried out in the T2 wind tunnel of ONERA Toulouse. T2 is a transonic, pressurized and cryogenic wind tunnel with closed circuit. The ONERA OAT15A airfoil was chosen with the "Trailing Edge Deflector" actuator (fig. 13). The 200 mm wing chord is equipped with 60 steady and 19 unsteady pressure transducers. The boundary layer transition is fixed at 7% of chord on upper and lower sides of the model. The tests were performed at ambient temperature with a chord Reynolds number of 4,5 millions and free stream Mach numbers between 0.72 and 0.78. The unsteady measurements were carried out simultaneously at a sampling rate of 15000 points per second and with a filtered signal of 5000 Hertz. The model structure was not subject to vibration. It was rigid and fixed to the test section walls.

The buffet onset can easily be detected by the pressure fluctuations levels measured on the upper side of the model, at the shock position or between the shock and the trailing edge. During buffet conditions, the measured signals are nearly periodical (fig. 10). The frequency, around 80 Hertz for this airfoil, depends on the model chord and on free stream flow conditions. The instantaneous position of the shock is deduced from the pressure measurements of the very closing transducers.

The deflector can be driven by dynamic movements around a static position. Various deflector motions in open loop (sinusoids, steps, phase shifts, etc.) were tested to try to understand the unsteady aerodynamic effect of the deflector with and without natural

buffet. Only transients realized with induced phase shifts (deflector angle/shock position) resulted in a short stabilization of the unsteady flow. In open loop with sine-shaped signals of deflector motions, the oscillation of the shock tends to become dependant on the deflector movement for some frequencies and amplitude. The oscillation of the shock becomes stronger and takes its movement frequency from the deflector. For flow conditions without natural buffet, it causes oscillations of the shock position for each amplitudes and frequencies. For flow conditions with natural buffet, it causes influenced buffet for certain amplitudes and frequencies of its motion. An influenced field and a synchronization threshold exist and depends on the natural buffet level and on the amplitudes and frequencies of the deflector motion (fig. 8). The buffet is dependent on the deflector motion. It is a very important result for dynamic control. An other important result for control is that the increase or the decrease of the deflector angle modifies the shock position. The shock position goes downstream with an increase of the deflector angle and vice versa.

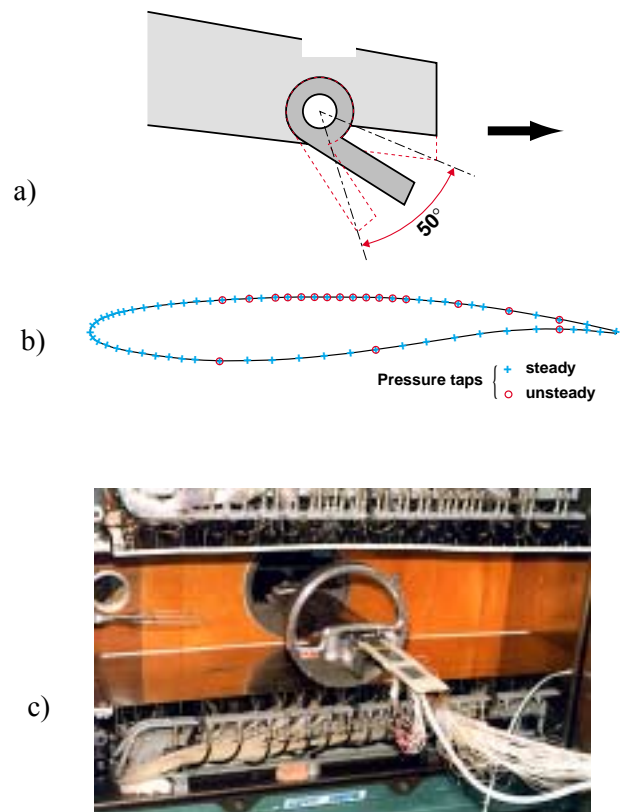


Fig. 13. a) The Trailing Edge Deflector.
b) The OAT15A airfoil and the instrumentation.
c) OAT15A model in T2 wind tunnel.

The open loop tests have shown that, for frequencies of the deflector motion near to buffet frequency, the deflector has a big influence in frequency, amplitude and phase on the shock position movement and on separation flow level. Buffet could only be stabilized with a closed loop approach, based on the unsteady measurements of the distribution of static pressure on the airfoil section. The idea is to move the deflector against the natural movement of the shock position. When the shock position wants to go upstream, the deflector angle is increased and vice versa. With the increase of the angle of attack for example, the shock goes downstream. Just at the buffet onset, it wants to go upstream ; it is the beginning of the shock position movement, the beginning of the buffet. The deflector angle is increased to force the shock to go downstream and vice versa. A control law has been found experimentally ; it agrees with the theoretical result of this study.

References

- [1] LE POURHIET A and LE MAITRE J.F. Une méthode générale d'étude de la stabilité d'un système non linéaire oscillant. *Int. J. Control*, 12, pp. 281-288, 1970.
- [2] LE POURHIET A and PAQUET J.G. Jump Phenomenon in a Van der Pol Oscillator. *Automatica*, vol. 7, pp. 481-487, 1971.
- [3] STOKER J.J. *Nonlinear vibrations*, pp. 147-187, Interscience, New York, 1966
- [4] HAYASHI C. *Non-linear oscillations in physical systems*, Mc Graw-Hill, New York, 1964.
- [5] GILLIES A.W. On the transformation of singularities and limit cycles of the variational equation of Van der Pol, *Q.J. Mech. Appl. Math.*, 7, part 2, 1954.
- [6] CARTWRIGHT M.L. Forced oscillations in nearly sinusoidal systems, *J. Inst. Elec. Eng. (London)* 95(3), 88-96, 1948.
- [7] DEWAN E.M. Harmonic entrainment of Van der Pol Oscillations : Phaselocking and Asynchronous Quenching, *IEEE Trans. Autom. Control*, Vol. AC-17, n°5, pp. 655-663, Oct. 1972.
- [8] LE POURHIET A. Comments on « Harmonic entrainment of Van der Pol Oscillations... », *IEEE Trans. Autom. Control*, Vol. AC-18, n°4, pp. 412-414, Aug. 1973.
- [9] GILLE J. Ch, DECAULNE P and PELEGRIN M. *Feedback Control Systems : Synthesis and Design*, Mc Graw-Hill, New York, 1958.
- [10] DESPRÉ C et al. Buffet active control : experimental and numerical results, *Symposium RTO, Active Control, Technology for enhanced performance operational capabilities of aircrafts*, Braunschweig, Germany May 2000.
- [11] CARUANA D et al. Buffet and buffeting active control, *AIAA, Fluids 2000*, June 2000, Denver, Co.
- [12] CARUANA D et al. *Contrôle actif des instabilités aérodynamiques à l'origine du tremblement. Ecoulement transonique bidimensionnel*. technical report. ONERA n° RF 1/5700.05-10-13 DMAE, 1998, Toulouse, France.
- [13] CARUANA D et al., Buffet and Buffeting Active Control with a Flap Actuator, *ICIASF*, Aug. 2001, Cleveland, USA.
- [14] GREITZER E. Surge and rotating stall in axial flow compressors, *ASME J. Eng. Power*, vol. 98, pp. 190-217, Apr. 1976.
- [15] GRAVDHAL J.T and EGELAND O. *Compressor surge and rotating stall, Modeling and Control*, Springer, 1998.
- [16] WILLEMS F and DE JAGER B. Modeling and Control of Compressor Flow Instabilities, *Control Systems Magazine*, vol. 19, n° 5, pp. 8-18, Oct.1999.
- [17] NELSON E.B, PADUANO J.D and EPSTEIN A.H. Active Stabilization of Surge in an Axicentrifugal Turboshaft Engine, *J. of Turbomachinery*, Vol. 122, n°. 3, July 2000.